

Integrated Pumped Hydro Reverse Osmosis System Optimization With Enhanced Reverse Osmosis Modeling

Matthew W. Haefner¹, Maha N. Haji^{2*}

¹ Department of Systems Engineering, Cornell University, United States

² Sibley School of Mechanical and Aerospace Engineering, Cornell University, United States

ABSTRACT

The pressure head generated by the upper reservoir of a pumped hydro energy storage system located at 500-700m elevation can also be sufficient for creating the pressure gradient required for a reverse osmosis desalination plant. Combined with the fact that many drought-stricken coastal areas have nearby mountains at the necessary elevation for these upper reservoirs, a symbiotic relationship can be ascertained through the co-location of a pumped storage hydropower (PSH) system with a reverse osmosis (RO) desalination system. Merging PSH and RO into one Integrated Pumped Hydro Reverse Osmosis (IPHRO) system [1] instead of implementing each individually could result in a number of benefits, including reduced capital investment, lower maintenance costs, and a natural mechanism for diluting the highly saline brine discharge generated from the RO process. This paper extends the work of Slocum et al. in 2016 [1], who first introduced IPHRO systems, by optimizing the amount of seawater diverted from the upper reservoir for energy recapture and fresh water production, respectively. For this multi-objective optimization, a new reverse osmosis model is created that utilizes a blend of empirical and fundamental equations based on the solution-diffusion model of membrane transport and boundary layer effects that naturally occur along reverse osmosis membranes. Doing so presents an attempt to increase the fidelity of the IPHRO system simulation model to better represent real-life scenarios, which will eventually aid in the IPHRO system's large-scale adoption into energy and freshwater infrastructures.

Keywords: Integrated Pumped Hydro Reverse Osmosis System, reverse osmosis, multidisciplinary design

Selection and peer-review under responsibility of the scientific committee of the 13th Int. Conf. on Applied Energy (ICAE2021).

Copyright © 2021 ICAE

optimization, solution-diffusion model, concentration polarization

NOMENCLATURE

<i>Abbreviations</i>	
IPHRO	Integrated Pumped Hydro Reverse Osmosis
RO	Reverse Osmosis
MDO	Multidisciplinary Design Optimization
<i>Symbols</i>	
A_w	Membrane water permeability coefficient [gfd/psi]
c_c	Concentrate salt concentration [mol/L]
c_f	Feed salt concentration [mol/L]
c_{fc}	Average salt concentration in RO element [mol/L]
c_m	Salt concentration along membrane [mol/L]
c_p	Permeate salt concentration [mol/L]
E_{er}	Total energy to consumer per day [kWh/day]
$E_{ht,RO}$	Energy from energy recovery per day [kWh/day]
E_r	Renewable energy generated per day [kWh/day]
E_{rd}	Energy sent directly to consumer per day [kWh/day]
E_{rp}	Energy to pump per day [kWh/day]
E_{swht}	Energy from turbine per day [kWh/day]
g	Gravitational constant [m/s ²]

h_L	Upper reservoir height [m]
M_{salt}	Molar mass of salt [g/mol]
N_e	Number of RO elements in series
N_{pv}	Number of RO pressure vessels in parallel
P_c	Concentrate pressure [psi]
P_f	Feed pressure [psi]
P_p	Permeate pressure [psi]
pf	Concentration polarization factor
Q_c	Concentrate flowrate [gpd]
Q_f	Feed flowrate [gpd]
Q_{fc}	Average flowrate in RO element [gpm]
Q_p	Permeate flowrate [gpd]
R	Fractional salt rejection rate
rr	Recovery ratio, individual RO element
S_{ht}	Discharge salinity [g/kg]
$S_{o,RO}$	Brine salinity [g/kg]
S_{sw}	Seawater salinity [g/kg]
SA	Membrane surface area [ft ²]
T	Temperature [°C]
$V_{fw,RO}$	Fresh water volume per day [m ³ /day]
V_{ht}	Discharge volume per day [m ³ /day]
$V_{o,RO}$	Brine volume per day [m ³ /day]
V_{swht}	Volume of water sent to turbine per day [m ³ /day]
V_{wp}	Volume of water pumped to upper reservoir per day [m ³ /day]
$V_{w,RO}$	Volume of water entering RO system per day [m ³ /day]
ΔP_{fc}	Pressure drop along RO element [psi]
γ	Fraction of E_r sent to IPHRO system
γ_{RO}	Fraction of seawater sent to RO system
η_{hp}	Pump-side efficiency
η_{ht}	Turbine-side efficiency
η_{RO}	Net RO recovery ratio
$\eta_{RO,io}$	Fraction of pressure leaving RO system
λ	Multi-objective weighting coefficient
π_f	Feed osmotic pressure [psi]
π_p	Permeate osmotic pressure [psi]
π_m	Osmotic pressure along membrane [psi]
ρ_{fw}	Fresh water density [kg/m ³]
ρ_{ht}	Discharge density [kg/m ³]
$\rho_{o,RO}$	Brine density [kg/m ³]
ρ_{sw}	Seawater density [kg/m ³]

1. INTRODUCTION

By the year 2050, demand for fresh water is expected to grow by over 40% [2]. This will increase the strain on a freshwater supply already being negatively impacted by factors such as droughts, increased urbanization, and an uneven distribution of freshwater resources [3,4]. A recent example highlighting this dire situation is the US Government declaring a water shortage at Lake Mead, a vital water source for the Southwestern United States, for the first time in the nation's history due to perpetuating drought conditions [5]. Reverse osmosis (RO) desalination plants are one means of increasing the freshwater supply by converting saline water, such as seawater, to drinking water. However, the energy requirement for pressurizing the RO process, if from fossil fuel sources, would only exacerbate the lack of fresh water due to the effects of global warming [6]. In comparison to the treatment of surface water for drinking water, which only requires 0.2-0.4 kWh/m³, the treatment of seawater for drinking water requires significantly more energy at 2.5-4 kWh/m³ [7]. Therefore, having the ability to incorporate renewable energy sources into the RO process would be ideal for eliminating the tradeoff between freshwater production from RO and carbon emissions from burning fossil fuels.

The potential energy of water stored in pumped storage hydropower systems is one means of creating the pressure gradient required for driving the RO process. While there are hundreds of examples of pumped hydro energy storage systems worldwide that, when combined, make up 97% of the world's large-scale energy storage, there are far fewer examples of significant pumped seawater hydro plants [8]. Conversely, seawater RO desalination has seen wide-scale implementation [9]. The fact that RO desalination plants and pumped hydropower plants can utilize and require elevated reservoirs respectively presents an opportunity for the co-location of these two systems as an Integrated Pumped Hydro Reverse Osmosis (IPHRO) system. This co-location factor provides many of the advantages IPHRO systems possess, as the sharing of infrastructures such as pumps and piping provides an opportunity for a reduction in capital investments and maintenance costs compared to if the two subsystems were implemented independently. Also, the utilization of the ocean provides a practically infinite source of water for RO and energy storage. Furthermore, co-location allows for easier dilution of the high salinity brine discharge from RO, as the mixing of the seawater stream from the pumped storage hydropower subsystem with

the brine stream prior to these streams entering the ocean reduces the salinity of the overall discharge compared to that of the brine stream salinity alone. This is important for mitigating adverse environmental effects and for regions that regulate the salinity of discharges into the ocean. These benefits could serve as incentives for governments to adopt these technologies.

Figure 1 shows a schematic of the IPHRO system, illustrating the flow of energy and water throughout the system. IPHRO systems were first proposed in the 2016 paper by Slocum et al. [1]. Since the emphasis of that paper was to show that IPHRO systems are feasible and to provide hypothetical results, there was no analysis of optimal operating conditions that maximize the amounts of fresh water and energy sent to the consumer. This paper undertakes initial efforts to find that optimal set by following multidisciplinary design optimization (MDO) principles. However, several simplifying assumptions were made in the initial model by [1], such as all-encompassing percentages, which gloss over real system complexities. Accordingly, this paper attempts to increase the IPHRO system model's fidelity to better emulate the real-life complexities of its subcomponents, in this case looking specifically at the RO module.

The performance metrics of RO membranes are commonly based on the solution-diffusion model for membrane flow [10], which expresses water and salt fluxes across the membrane as a function of concentration gradients, pressures, and osmotic pressures. This mass transport is difficult to model. Consequently, the seemingly standard convention for authors across the literature is to make varying degrees of assumptions and make use of the commercially available RO design software WAVE [11] in the calculation of membrane properties and the development of their own models. In this paper, a new RO model for incorporation into the IPHRO system is detailed, which solves for the permeate flowrate within the overarching MDO framework, utilizes WAVE in the development of equations for the fractional salt rejection rate R and the membrane water permeability constant A_w , and is based on the solution-diffusion model with consideration of concentration polarization effects that occur along the surface of the RO membrane. Additionally, initial results from optimizing the IPHRO system model with the new RO model are presented.

2. IPHRO SYSTEM MODEL

An overview of the IPHRO system simulation model is detailed in the block diagram shown below in Figure 2. Due to space constraints, a full main table listing all

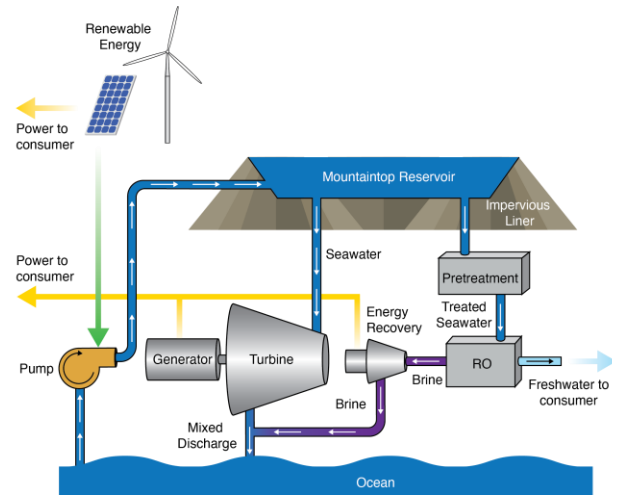


Fig. 1. Schematic of IPHRO system.

variables relevant to IPHRO systems and their assignment to design, constraint, objective, parameter, and dependent variables is not included in this paper. The governing equations for the IPHRO system are detailed in this section.

Equations for the density and salinity of the discharge from the IPHRO system into the ocean are derived from conservation of mass analyses on the salt and pure water mass flowrates into and out of the Mixture and RO System modules:

$$S_{ht} = \frac{S_{sw}\rho_{sw}}{\rho_{sw} - \gamma_{RO}\eta_{RO}\rho_{fw}} \quad (1)$$

$$\rho_{ht} = \frac{\rho_{sw} - \gamma_{RO}\eta_{RO}\rho_{fw}}{1 - \gamma_{RO}\eta_{RO}} \quad (2)$$

The energy sent to the pump, E_{rp} , can be expressed either in terms of E_r or the potential energy of V_{wp} in the upper reservoir, accounting for losses on the pump-side of the IPHRO system, which is assumed to be constant at $\eta_{hp} = 89.4\%$:

$$E_{rp} = \gamma E_r = \frac{\rho_{sw} V_{wp} g h_L}{\eta_{hp} * 3.6 \times 10^6} \quad (3)$$

Solving for E_r provides the key equation relating energy quantities in the model to water quantities:

$$E_r = \frac{\rho_{sw} g h_L}{\gamma \eta_{hp} * 3.6 \times 10^6} V_{wp} \quad (4)$$

The total energy to the consumer is given by the sum of E_{rd} , E_{swht} , and E_{htRO} :

$$E_{er} = (1 - \gamma)E_r + (1 - \gamma_{RO})\gamma\eta_{hp}\eta_{ht}E_r + \left(1 - \eta_{RO} \frac{\rho_{fw}}{\rho_{sw}}\right)\gamma\gamma_{RO}\eta_{RO,io}\eta_{hp}\eta_{ht}E_r \quad (5)$$

where the turbine-side efficiency η_{ht} is also assumed to be constant at 89.4%.

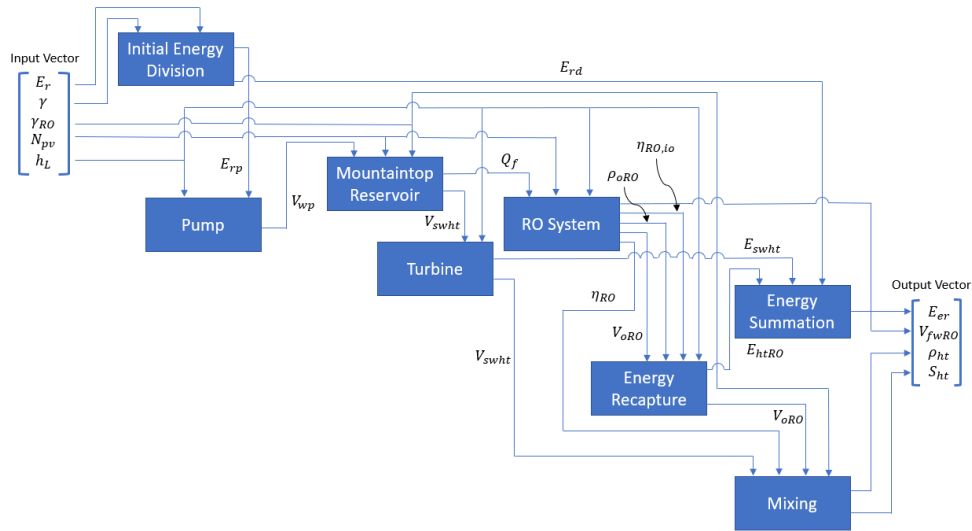


Fig. 2. Block diagram of the IPHRO system model.

3. NEW RO MODEL

3.1 RO theory overview

A wide variety of membrane transport models have been developed to characterize the flow of water and solutes across osmosis membranes [12]. Of these models, the solution-diffusion model has been utilized frequently throughout the literature. A complete review of the solution-diffusion model has previously been conducted in [10].

A significant factor in the realization of flowrates across RO membranes that the solution-diffusion model does not account for is boundary layer effects along the feed side of the membrane. This phenomenon is referred to as concentration polarization. As seawater diffuses across the membrane, the salt in the seawater does not enter the membrane as readily as the water does. This difference creates a concentration gradient between the boundary layer region adjacent to the membrane and the main feed flow, resulting in salt diffusion away from

the membrane, hindering flowrates across the membrane [13]. Assuming steady state allows for the salt concentration at the feed side of the membrane to be known. Figure 3 shows approximate profiles of the water and salt concentrations inside and near the membrane.

3.2 Governing equations

Below are the key governing equations which define this RO model. From [10], the quintessential equation for characterizing RO permeate flow for the solution-diffusion model is obtained by equating the chemical potentials at each water-membrane interface and utilizing Fick's first law of diffusion. The resulting equation is shown below in Equation 6:

$$Q_p = A_w(SA) \times \left(P_f - \frac{\Delta P_{fc}}{2} - P_p - \pi_m + \pi_p \right) \quad (6)$$

Equation 6 assumes that there is no membrane fouling, which would inhibit flow across the membrane, and that the temperature is standard at 25°C. Otherwise, there would be additional fouling factors and temperature correction factors to include in Equation 6 [14].

For applications to the reverse osmosis of seawater, the following equation is a widely used approximation for calculating the osmotic pressure [13]:

$$\pi_{region} = 1.12(273 + T) \sum \bar{m}_{i,region} \quad (7)$$

where \bar{m}_i is the molarity of a dissolved ionic or nonionic species in a solution and the region subscript refers to the feed region (f), permeate region (p), etc. However, assuming that the salt in seawater is strictly NaCl and with concentrations in this paper being defined in mol/L, Equation 7 simplifies to

$$\pi_{region} = 1.12(273 + T)(2c_{region}) \quad (8)$$

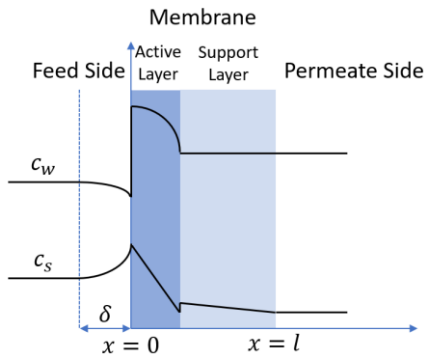


Fig. 3. Water and salt concentration profiles close to and within the RO membrane, incorporating boundary layer δ . Adapted from [13]. Profiles are approximate.

The FilmTec™ Seamaxx™-440 Element RO membrane made by Dupont is used in this analysis due to its significantly higher flowrates than other seawater RO membranes and therefore its lower energy consumption [15]. For 8-inch FilmTec™ membranes, the concentration polarization factor pf and the pressure drop along an RO element ΔP_{fc} can be approximated by [14]:

$$pf = \exp(0.7rr) \quad (9)$$

$$\Delta P_{fc} = 0.01Q_{fc}^{1.7} \quad (10)$$

The membrane water permeability coefficient A_w and the fractional salt rejection rate R are both parameters intrinsic to the membrane, as they characterize the transport of mass across the membrane. Typically, these variables are calculated experimentally [12], though a suitable alternative is achieved by running experimental simulations through the WAVE design software. These simulations were run for three Seamaxx™-440 elements in series in one pressure vessel, with the permeate flowrate through the first membrane kept at the highest possible value of 1.32 m³/hr. Additionally, the total system recovery was set at 25%, which allowed for a full sweep of the feed salinity from 1000 mg/L to 40000 mg/L while remaining within the design limits of the membrane, which are detailed later in this paper. As the feed salinity was increased, the feed flowrate was decreased to keep the same maximum allowable permeate flowrate going through the first membrane. Fitting second order polynomial equations to the resulting data from WAVE results in Equations 11, which express A_w as a function of the osmotic pressure along a membrane:

$$A_w(\pi_m) = 4.457 \times 10^{-8}\pi_m^2 - 1.7765 \times 10^{-4}\pi_m + 0.1694 \quad (11)$$

and Equation 12, which expresses R as a function of the permeate flowrate through a membrane:

$$R(Q_p) = -1.6615 \times 10^{-10}Q_p^2 + 3.2118 \times 10^{-6}Q_p + 0.9789 \quad (12)$$

As this model currently stands, it will be assumed that changing the net system recovery does not alter these two equations. In reality, A_w and R are susceptible to changes in η_{RO} , but these changes are minimal. What is arguably more important here is encapsulating the trends in these variables as the operating conditions are changed.

The feed salt concentration for the first RO element can be derived from known quantities by dimensional analysis:

$$c_f = \frac{S_{sw}\rho_{sw}}{1000M_{salt}} \quad (13)$$

The permeate salt concentration for each individual element is related to the fractional salt rejection rate by Equation 14:

$$c_p = c_f(1 - R) \quad (14)$$

The following equation for the concentrate salt concentration is derived from a conservation of mass analysis on an RO element, solving for the salt concentration of the concentrate discharge from an RO element:

$$c_c = \frac{Q_f c_f - Q_p c_p}{Q_c} \quad (15)$$

where Q_c is simply the difference between the feed flowrate and permeate flowrate for an RO element.

The average salt concentration in the bulk flow along the length of an RO element is simply approximated as a linear average of the inlet and outlet salt concentrations of an RO element:

$$c_{fc} = \frac{c_f + c_c}{2} \quad (16)$$

A similar approach can be taken for the average flowrate of the bulk flow along the length of an RO element, making note of the gpm units required for use in Equation 10:

$$Q_{fc} = \frac{Q_f + Q_c}{2 * 1440} \quad (17)$$

While Equation 9 already defines pf as a function of rr , pf can also be expressed as the ratio of the difference in salt concentrations between the membrane surface and the permeate to the difference in salt concentrations between the bulk flow and the permeate [16]. This equation can then be rearranged to provide an equation for the salt concentration along the membrane:

$$c_m = pf(c_{fc} - c_p) + c_p \quad (18)$$

The recovery ratio for an element, rr , is defined as the permeate flowrate divided by the feed flowrate:

$$rr = \frac{Q_p}{Q_f} \quad (19)$$

Lastly, the pressure of the concentrate flow leaving an RO element is the difference between the feed pressure and the pressure drop that occurs along the length of an RO element:

$$P_c = P_f - \Delta P_{fc} \quad (20)$$

3.3 Assumptions

A list of the assumptions that are made in this model, which have not been noted already, are:

- $P_p = 14.696$ psi (1 atm)
- $S_{sw} = 35$ g/kg
- $\rho_{sw} = 1023.6$ kg/m³
- $\rho_{fw} = 996.9$ kg/m³
- $T = 25^\circ\text{C}$

- $M_{\text{salt}} = 58.44 \text{ g/mol}$
- $N_e = 3$

One thing to note is that ρ_{fw} does not refer to the density of the permeate flow, since there are still slight quantities of salt that pass through the membrane. Those densities will be incorporated into the model in future work.

3.4 SeamaxTM-440 element properties

- $0 \leq rr \leq 0.13$
- $3.41 \text{ m}^3/\text{hr} \leq Q_f \leq 15.5 \text{ m}^3/\text{hr}$
- $0 \leq Q_p \leq 1.32 \text{ m}^3/\text{hr}$
- $A_m = 440 \text{ ft}^2$

3.5 RO model algorithm

For a given P_f and Q_f , with S_{sw} , ρ_{sw} , and Q_p known for the first RO element, all other RO variables can be directly calculated. From this first RO element, P_c , Q_c , and c_c become P_f , Q_f , and c_f respectively for the next RO element. Q_p is then solved for symbolically. This process is carried out for all additional elements in the pressure vessel. As the model currently stands, the number of RO elements in series, N_e , is kept constant at three, but will become a design variable in future work.

3.6 Incorporation into IPHRO model

As noted in Figure 2, the five design variables in the IRPHO system model are E_r , γ , γ_{RO} , N_{pv} , and h_L . With $V_{\text{w,RO}}$ being a fraction, γ_{RO} , of V_{wp} , $V_{\text{w,RO}}$ can then be expressed in terms of design variables by use of Equation 4:

$$V_{\text{w,RO}} = \frac{3.6 \times 10^6 * E_r \gamma \gamma_{\text{RO}} \eta_{\text{hp}}}{\rho_{\text{sw}} g h_L} \quad (21)$$

Since there is a maximum limit to the feed flowrate each pressure vessel making up the RO system can allow, dividing $V_{\text{w,RO}}$ by N_{pv} allows for the feed flowrate into each pressure vessel to be expressed in terms of overarching design variables:

$$Q_f = \frac{3.6 \times 10^6 * E_r \gamma \gamma_{\text{RO}} \eta_{\text{hp}} * 264.172}{\rho_{\text{sw}} g h_L N_{\text{pv}}} \quad (22)$$

The total volume per day of fresh water generated from the RO system can be calculated by the summation of the permeate flow rates from each individual element multiplied by the number of pressure vessels in the RO system:

$$V_{\text{fwRO}} = N_{\text{pv}} \sum_{i=1}^{N_e} \frac{Q_{p,i}}{264.172} \quad (23)$$

and the total volume per day of brine generated from the RO system can be calculated by the summation of the concentrate flowrates exiting each pressure vessel:

$$V_{\text{oRO}} = N_{\text{pv}} * \frac{Q_{c,\text{last element}}}{264.172} \quad (24)$$

Additionally, the feed pressure for the first element of a pressure vessel is directly related to the height of the upper reservoir by the following conversion equation:

$$P_f = 0.0981 * h * \frac{\rho_{\text{sw}}}{\rho_{\text{fw}}} * 14.504 \quad (25)$$

Equation 25 assumes that there are no frictional losses to $V_{\text{w,RO}}$ prior to the stream entering the RO system.

Furthermore, the net RO recovery ratio can be calculated from the individual recoveries for each element by:

$$\eta_{\text{RO}} = 1 - \prod_{i=1}^{N_e} (1 - rr_i) \quad (26)$$

and the fraction of pressure leaving the RO system can be calculated from the pressures computed in the RO model:

$$\eta_{\text{RO,io}} = 1 - \frac{P_{f,1\text{st element}} - P_{c,\text{last element}}}{P_{f,1\text{st element}}} \quad (27)$$

Lastly, correlation equations, detailed in [17], allow for the salinity to be calculated from the osmotic pressure, and the density to then be calculated from the salinity, at elevated pressures. These correlations are used to determine $S_{\text{o,RO}}$ and $\rho_{\text{o,RO}}$.

4. IPHRO SYSTEM MODEL OPTIMIZATION

4.1 Objectives and constraints

Looking at the model holistically, it is clear that there are two competing objectives, E_{er} and V_{fwRO} , which are desired to be maximized. These objectives are dictated by the values of the design variables E_r , γ , γ_{RO} , N_{pv} , and h_L .

The primary constraint in this model, as it currently stands, is the salinity (and density) of the final discharge into the ocean, S_{ht} and ρ_{ht} respectively. These variables are related in that they both represent the concentration of salt in the final discharge. For this model however, both are expressed due to their applicability to different equations. Different regions of the world have different requirements on the salinity of brine discharged into the ocean to mitigate adverse environmental effects. For instance, California sets an upper limit to discharge salinity at 40 grams of salt per kilogram of seawater [18]. California's discharge salinity limit is the constraint adopted in this paper.

Additional constraints arise from the RO model. As noted in Section 3.4, there are design limits to rr , Q_f , and Q_p for the Seamaxx™-440 element, but also more generally for any RO element. As the optimization algorithm runs, any time that the value of one of these constraints is violated, the responsible design variable configuration is instantly deemed infeasible, and returns a sufficiently large objective value to not be deemed remotely optimal.

4.2 Formal problem statement

Expressing this MDO problem in standard form results in the following problem statement:

$$\begin{aligned} \min \quad & J(x, p) \\ \text{s.t.} \quad & S_{ht} - 40 \leq 0 \\ & -rr \leq 0 \\ & rr - 0.13 \leq 0 \\ & 3.41 - Q_f \leq 0 \\ & Q_f - 15.5 \leq 0 \\ & -Q_p \leq 0 \\ & Q_p - 1.32 \leq 0 \\ & \begin{bmatrix} 0 \\ 0.01 \\ 0.01 \\ 274 \\ 1 \end{bmatrix} \leq \begin{bmatrix} E_r \\ \gamma \\ Y_{RO} \\ h_L \\ N_{pv} \end{bmatrix} \leq \begin{bmatrix} 100 \times 10^6 \\ 0.99 \\ 0.99 \\ 550 \\ 1000 \end{bmatrix} \end{aligned}$$

where

$$J = \lambda(-V_{fWRO}) + (1 - \lambda)(-E_{er})$$

Making the objectives negative in J effectively maximizes these two variables in the optimization algorithm. h_L being in the range of 274 meters and 550 meters correlates to a feed pressure range of approximately 400 psi and 800 psi based on Equation 25.

4.3 Optimization results

Optimization was completed heuristically using a multi-objective genetic algorithm, specifically a variant of NSGA-II utilized by the gamultiobj MATLAB function [19]. The population size was set to 200, and the crossover fraction was set to 0.9. All other options were kept at default values.

Figure 4 shows the resulting Pareto front from the above optimization. Prior to the development of the RO model presented in this paper, the Pareto front generated was linear due to a linear dependence that was later realized between E_{er} and V_{fWRO} . Conversely, the new optimization results clearly show a distinct tradeoff between only optimizing for maximum E_{er} and only optimizing for maximum V_{fWRO} , as well as a distinct “elbow” in the Pareto front, which can be interpreted as a sweet spot for maximal values of both objectives.

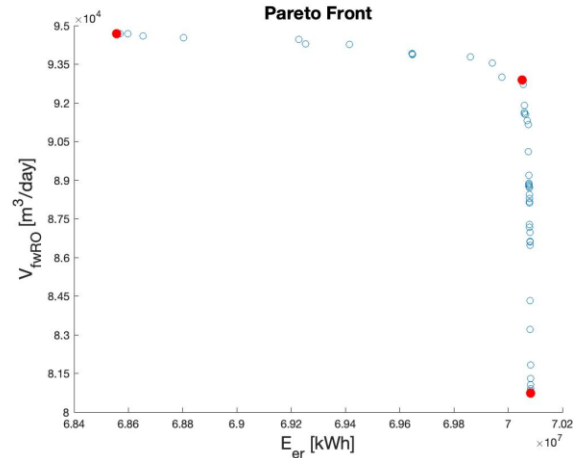


Fig. 4. Pareto front created by use of a genetic algorithm used to maximize V_{fWRO} and E_{er} . The Pareto points indicated by red markers are highlighted in Table 1.

A comparison of the Pareto points that most maximize E_{er} , most maximize V_{fWRO} , and relatively maximizes both objectives, indicated as red points in Figure 4, is shown below in Table 1. At the relatively maximum combination of E_{er} and V_{fWRO} (on the “elbow” of the Pareto front), there is a 0.0428% decrease from the maximum possible E_{er} and a 1.91% decrease from the maximum possible V_{fWRO} , compared to a 2.18% increase in the E_{er} at maximum V_{fWRO} and a 15.0% increase in the V_{fWRO} at maximum E_{er} . This signifies that by sacrificing slightly from the maximum possible E_{er} and V_{fWRO} values, one can still see relatively large amounts of fresh water and energy being delivered to the consumer.

Table 1: Comparison of select Pareto points shown in Figure 4.

Pareto Point →	@ max(E_{er})	@ max(V_{fWRO})	@ rel. max(E_{er}, V_{fWRO})
E_{er} Value	7.0082×10^7	6.8556×10^7	7.0052×10^7
V_{fWRO} Value	8.0744×10^4	9.4687×10^4	9.2883×10^4
x^*	$[7.0096 \times 10^7]$	$[6.9067 \times 10^7]$	$[7.0088 \times 10^7]$
$= \begin{bmatrix} E_r^* \\ \gamma^* \\ Y_{RO}^* \\ h_L^* \\ N_{pv}^* \end{bmatrix}$	$\begin{bmatrix} 0.037601 \\ 0.18404 \\ 508.47 \\ 829 \end{bmatrix}$	$\begin{bmatrix} 0.078251 \\ 0.10418 \\ 526.56 \\ 918 \end{bmatrix}$	$\begin{bmatrix} 0.043768 \\ 0.17981 \\ 522.09 \\ 921 \end{bmatrix}$

5. CONCLUSIONS

Developing a new RO model for the IPHRO system detailed in this paper represents an initial venture into

increasing the accuracy of the IPHRO system model in representing real-life phenomena. The tradeoff that exists between the amount of energy delivered to the consumer and the amount of fresh water delivered to the consumer from this IPHRO system model should be considered when implementing an IPHRO system in actuality. Future work will include considerations such as modeling the flow of seawater throughout the entire IPHRO system, the mixing of the seawater and brine streams prior to their combined discharge into the ocean, and incorporating consumer demand models into the IPHRO system model.

ACKNOWLEDGEMENT

This work was supported in part by the McMullen Graduate Fellowship for first year doctoral students via Cornell University's Systems Engineering Department.

REFERENCE

- [1] Slocum, A. H., Haji, M. N., Trimble, A. Z., Ferrara, M., & Ghaemsaïdi, S. J. (2016). Integrated Pumped Hydro Reverse Osmosis Systems. *Sustainable Energy Technologies and Assessments*, 18, 80–99. <https://doi.org/10.1016/j.seta.2016.09.003>
- [2] Eliasson, J. (2014). The rising pressure of global water shortages. *Nature*, 517(7532), 6–6. <https://doi.org/10.1038/517006a>
- [3] United Nations Department of Economic and Social Affairs. (2014, November 24). *Water and cities*. Retrieved November 17, 2021, from https://www.un.org/waterforlifedecade/water_cities.shtml.
- [4] Rogers, P. (2008). Facing the freshwater crisis. *Scientific American*, 299(2), 46–53. <https://doi.org/10.1038/scientificamerican0808-46>
- [5] Fountain, H. (2021, August 16). In a First, U.S. Declares Shortage on Colorado River, Forcing Water Cuts. *The New York Times*. Retrieved November 17, 2021, from <https://www.nytimes.com/2021/08/16/climate/colorado-river-water-cuts.html>.
- [6] Gillis, J. (2015, August 20). California Drought Is Made Worse by Global Warming, Scientists Say. *The New York Times*. Retrieved November 17, 2021, from <https://www.nytimes.com/2015/08/21/science/climate-change-intensifies-california-drought-scientists-say.html>.
- [7] Kim, J., Park, K., Yang, D. R., & Hong, S. (2019). A comprehensive review of energy consumption of seawater reverse osmosis desalination plants. *Applied Energy*, 254, 113652. <https://doi.org/10.1016/j.apenergy.2019.113652>
- [8] Australian Government. (2017). (rep.). *Cultana Pumped Hydro Project Knowledge Sharing Report*. Retrieved November 17, 2021, from https://arena.gov.au/assets/2017/09/Cultana-Pumped-Hydro-Project_Public-FINAL-150917.pdf.
- [9] Faigon, M. (2016). Success Behind Advanced Swro Desalination Plant. *Filtration + Separation*, 53(3), 29–31. [https://doi.org/10.1016/s0015-1882\(16\)30121-5](https://doi.org/10.1016/s0015-1882(16)30121-5)
- [10] Wijmans, J. G., & Baker, R. W. (1995). The solution-diffusion model: A review. *Journal of Membrane Science*, 107(1-2), 1–21. [https://doi.org/10.1016/0376-7388\(95\)00102-i](https://doi.org/10.1016/0376-7388(95)00102-i)
- [11] WAVE Design Software. (n.d.). Version (1.77). *DuPont Water Solutions*. Retrieved October 6, 2020, from <https://www.dupont.com/water/resources/design-software.html>.
- [12] Wang, J., Dlamini, D. S., Mishra, A. K., Pendergast, M. T., Wong, M. C. Y., Mamba, B. B., Freger, V., Verliefe, A. R. D., & Hoek, E. M. V. (2014). A critical review of transport through osmotic membranes. *Journal of Membrane Science*, 454, 516–537. <https://doi.org/10.1016/j.memsci.2013.12.034>
- [13] Seader, J. D., & Henley, E. J. (2006). *Separation process principles* (2nd ed.). John Wiley & Sons.
- [14] DuPont Water Solutions. (2021, September). *Filmtec reverse osmosis membranes technical manual*. Retrieved November 17, 2021, from <https://www.dupont.com/content/dam/dupont/amer/us/en/water-solutions/public/documents/en/45-D01504-en.pdf>.
- [15] *Filmtec™ Seamaxx™-440 element*. DuPont Product Data Sheet. (2021, August). Retrieved November 17, 2021, from <https://www.dupont.com/content/dam/dupont/amer/us/en/water-solutions/public/documents/en/45-D00689-en.pdf>.
- [16] Okamoto, Y., & Lienhard, J. H. (2019). How RO membrane permeability and other performance factors affect process cost and energy use: A Review. *Desalination*, 470, 114064. <https://doi.org/10.1016/j.desal.2019.07.004>
- [17] Nayar, K. G., Sharqawy, M. H., Banchik, L. D., & Lienhard V, J. H. (2016). Thermophysical properties of seawater: A review and new correlations that include pressure dependence. *Desalination*, 390, 1–24. <https://doi.org/10.1016/j.desal.2016.02.024>
- [18] Jenkins, S., Paduan, J., Roberts, P., Schlenk, D., & Weis, J. (2012). (tech.). *Management of brine discharges to coastal waters: recommendations of a science*

advisory panel. Southern California Coastal Water Research Project. Retrieved November 17, 2021, from https://www.waterboards.ca.gov/water_issues/programs/ocean/desalination/docs/dpr051812.pdf

[19] MathWorks. (n.d.). gamultiobj Algorithm. Retrieved January 18, 2022, from <https://www.mathworks.com/help/gads/gamultiobj-algorithm.html>